

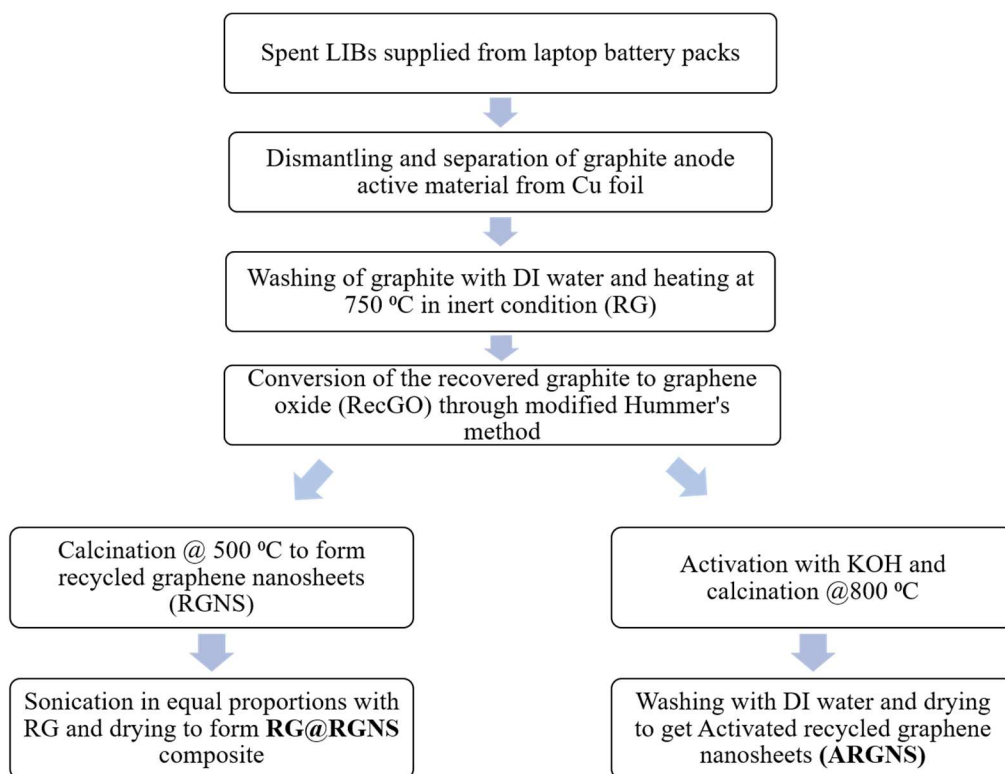
## Supplementary Material

### Upcycling of Spent Lithium-ion Battery Graphite Anodes for Dual Carbon Lithium-ion Capacitor

*Udita Bhattacharjee, Madhushri Bhar, Subhajit Bhowmik, and Surendra K Martha\**

Department of Chemistry, Indian Institute of Technology Hyderabad, Kandi, Sangareddy, 502284, Telangana, India

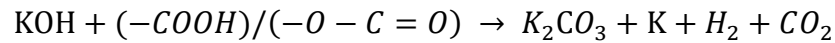
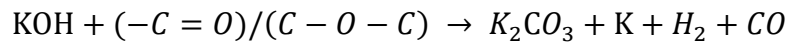
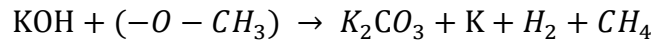
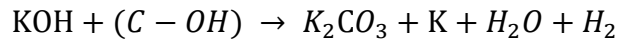
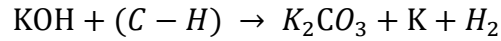
\* Corresponding author. E-mail: martha@chy.iith.ac.in



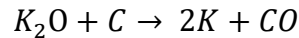
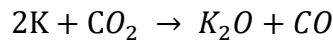
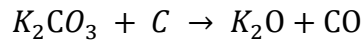
*Supplementary Scheme S1: A flowchart showing the recovery of raw material and electrode active material synthesis methodology.*

The reactions involved in the KOH activation process of the carbon matrix are given below.

At a temperature range of 400-600 °C:



At temperatures  $\geq 800$  °C:



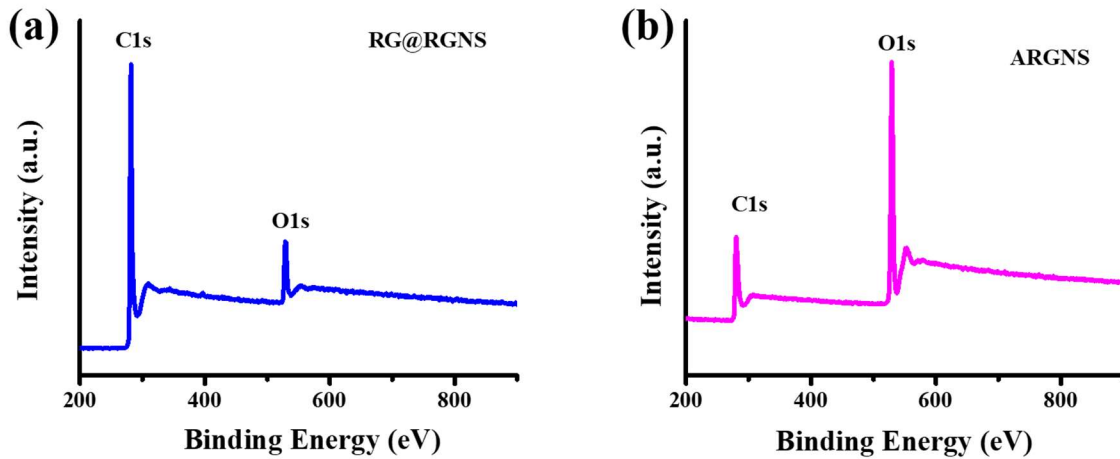
### Formulae for Specific Power and Specific Energy calculation:

The specific capacitances from the GCD curves were calculated using the formula

$$\text{Specific Capacitance (F/g)} = \frac{\text{Current, } i(\text{A}) * \text{Time of discharge, } t(\text{s})}{\text{Voltage difference, } dV(\text{V}) * \text{Active mass, } m(\text{g})} = \frac{\text{Sp. capacity } \left(\frac{\text{mAh}}{\text{g}}\right) * 3600}{1000 * dV(\text{V})}$$

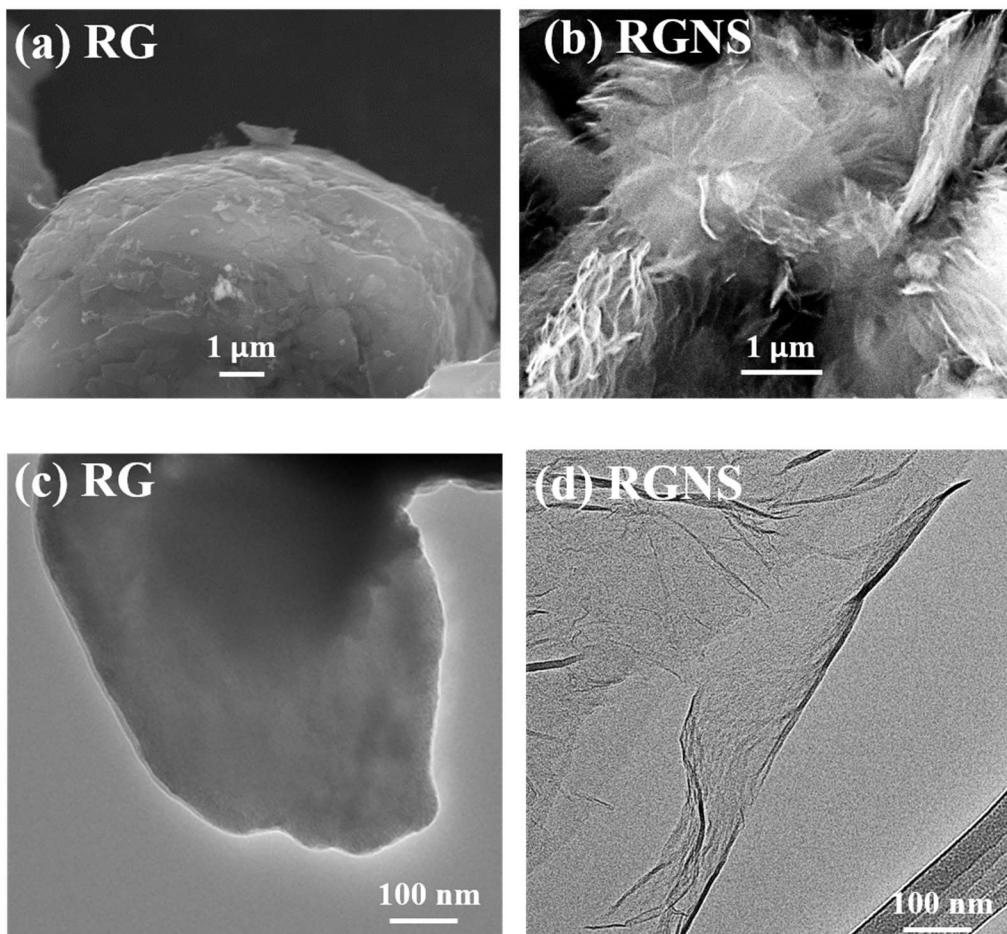
The cycling stabilities were studied at  $1 \text{ Ag}^{-1}$  current density. The energy-power output relationship of the LIC cells developed was analyzed through the Ragone plot at a coin cell level, considering both electrode active masses only. The specific power ( $P_s$ ) and specific energy ( $E_s$ ) were calculated using the formulae  $P_s = \frac{V \cdot I}{M}$  and  $E_s = P_s \cdot t$ , respectively where  $V = \frac{V_{max} + V_{min}}{2}$  in Volts,  $I$  is the current applied in A,  $M$  is the active mass of both electrodes in kg, and  $t$  is the time in hours.

The volumetric power density ( $P_v$ ) and energy density ( $E_v$ ) are calculated using the formulae  $P_v = \frac{V \cdot I}{\text{Volume of both electrode coating}}$  and  $E_v = P_v \cdot t$ .



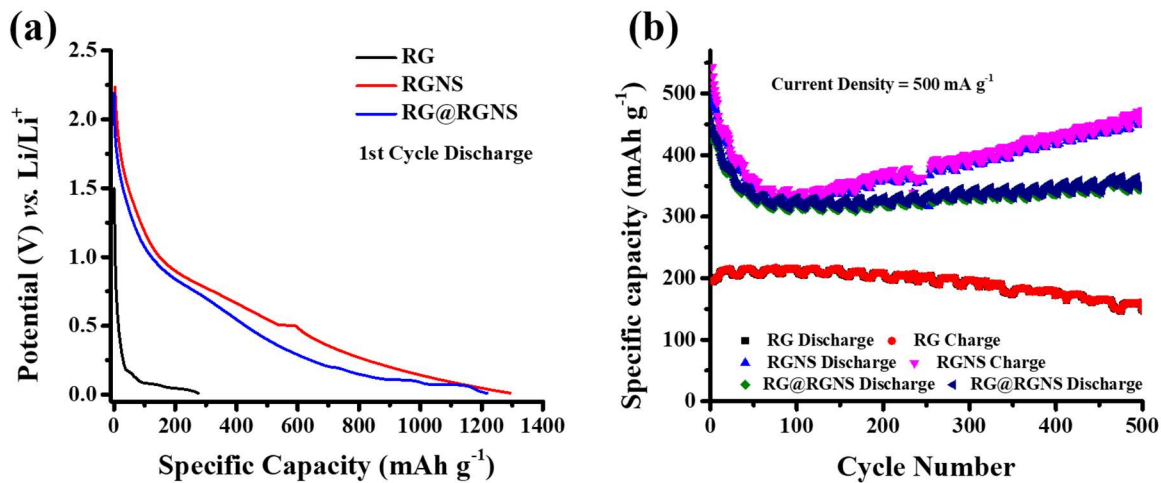
**Supplementary Figure S1:** XPS survey scan of (a) RG@RGNS, and (b) ARGNS

The survey scan of RG@RGNS (Supplementary Figure S1) shows the elemental composition of the matrix as 89.4% carbon and 10.6% oxygen. Further, the survey scan (Supplementary Figure S1) shows a presence of 57 % carbon and 43 % oxygen in the ARGNS matrix.



**Supplementary Figure S2:** (a-b) SEM and (c-d) TEM images of RG and RGNS.

The SEM and TEM images of RG show graphitic microstructures with layered arrangements. At the same time, a disordered array of nanosheets is visualized in the case of RGNS.

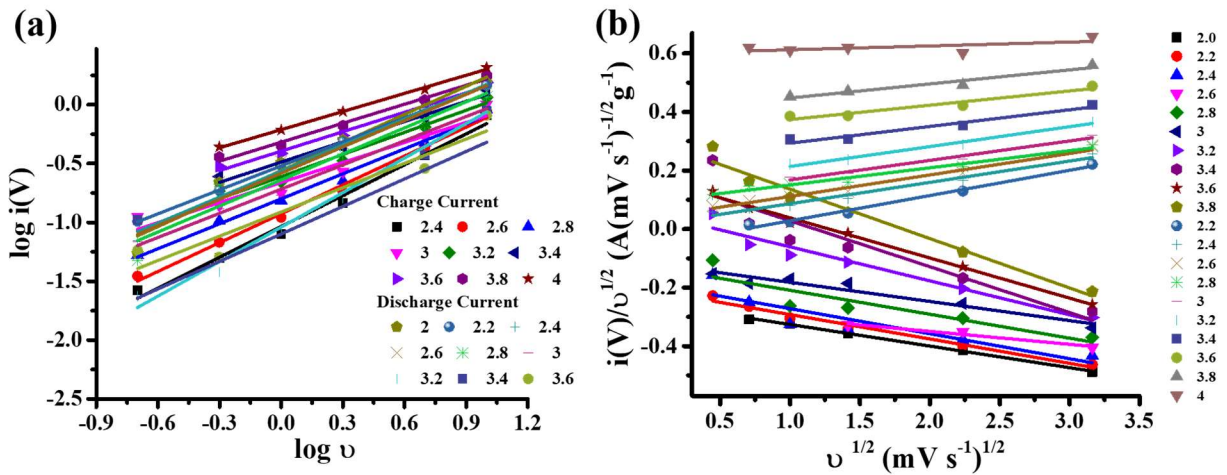


**Supplementary Figure S3:** (a) Voltage profile, and (b) Cycling stability at 500 mA g<sup>-1</sup> comparison of anode half cell of RG, RGNS, and RG@RGNS vs. Li/Li<sup>+</sup>.

The comparative discharge voltage profiles of RG, RGNS, and RG@RGNS are shown in Supplementary Figure S3a, which provides an insight into their relative Li-ion storage phenomenon.

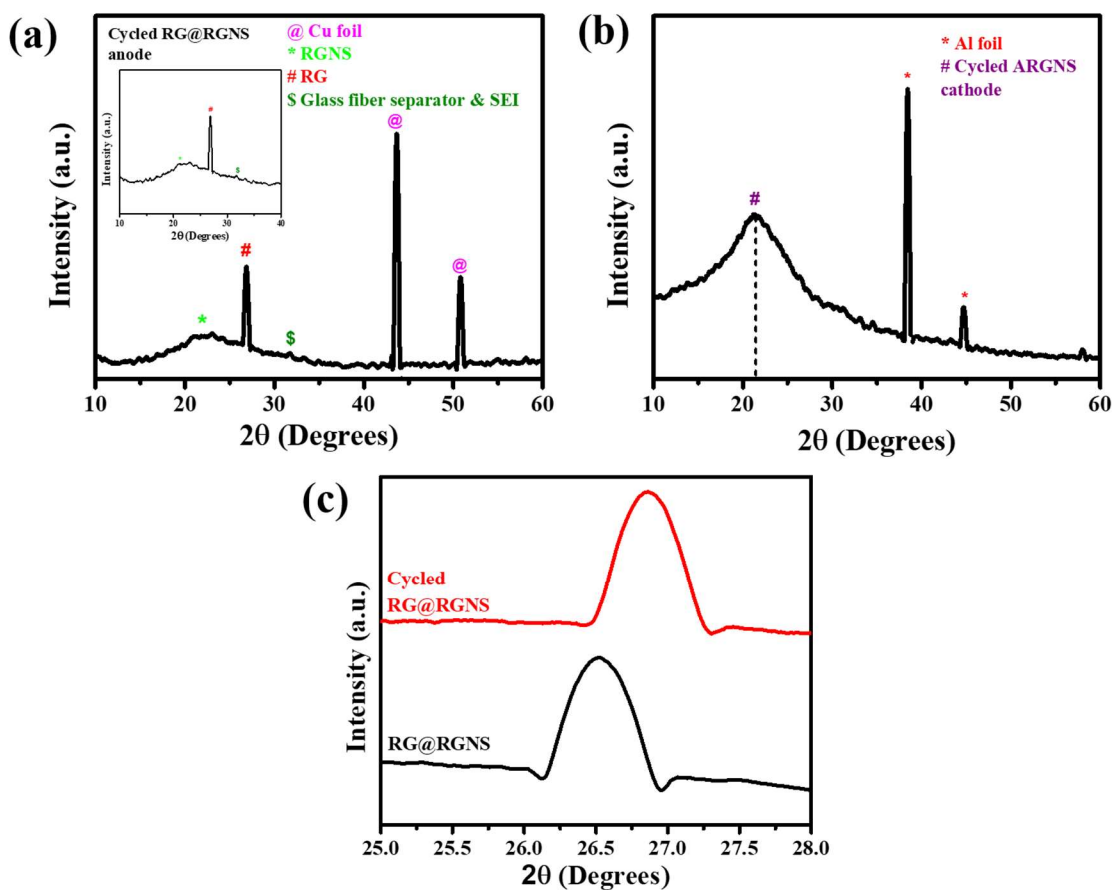
RG@RGNS delivers a capacity of 320 mAh g<sup>-1</sup> at a current density of 1 A g<sup>-1</sup> till 1000 cycles (Figure 5f). RG@RGNS, when subjected to different current rate cycling (Figure 5g) from 0.1 A g<sup>-1</sup> to 10 A g<sup>-1</sup>, it is found to deliver a specific capacity of 120 mAh g<sup>-1</sup> at a high current density of 5 A g<sup>-1</sup>.

RG, RGNS, and RG@RGNS electrodes, when cycled at a current density of 500 mAh g<sup>-1</sup>, deliver a specific capacity of 180, 480, and 350 mAh g<sup>-1</sup>, respectively (Supplementary Figure S3b) for 500 cycles.



**Supplementary Figure S4:** (a)  $\log i(V)$  vs.  $\log v$  plot, and (b)  $i(V)/v^{1/2}$  vs.  $v^{1/2}$  plot of pre-lithiated RG@RGNS full cell at different potentials during an anodic and cathodic scan of cyclic voltammogram in the potential range 2.0-4.0 V.

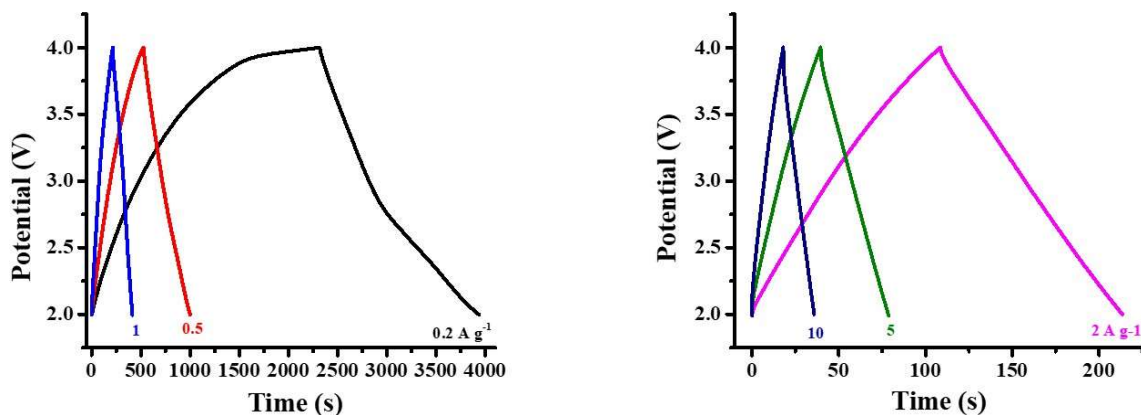
The capacitive and diffusive current contribution at a particular voltage at varying potential rates were analyzed through the Trassati procedure by using the equation,  $i(V) = k_1 * v + k_2 * v^{1/2}$ , where  $i$  = current at voltage  $V$ ,  $k_1 * v$  = capacitive component and  $k_2 * v^{1/2}$  = diffusive component. [1] Analyzing the  $i(V)/v^{1/2}$  versus  $v^{1/2}$  plot (Supplementary Figure S4b), both capacitive and diffusive components in the current response were quantified.



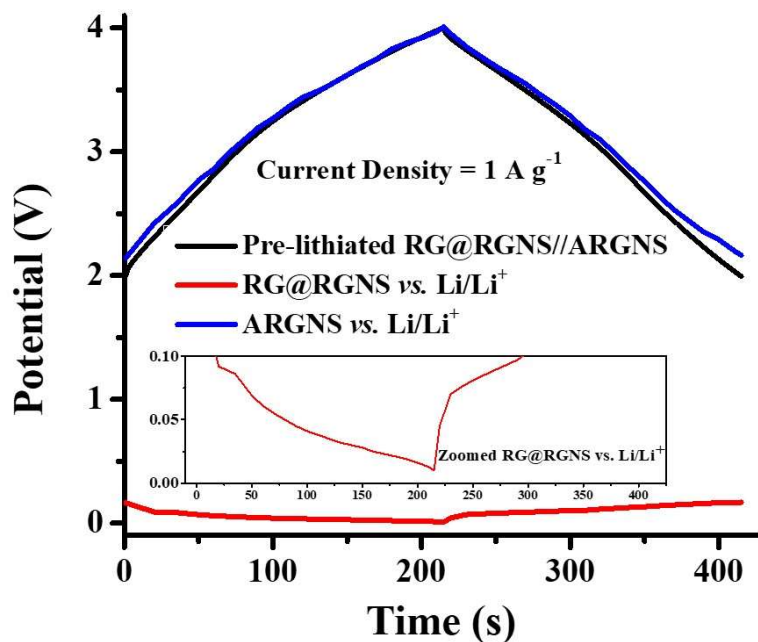
**Supplementary Figure S5:** Ex-situ postmortem XRD for cycled (a) RG@RGNS anode and (b) ARGNS cathode. (c) Comparison plot of the graphitic peak of RG@RGNS composite between pristine and cycled anode.

The post-cycling ex-situ XRD of both the electrodes indicates the interlayer rearrangement in the case of RG@RGNS anode and ARGNS cathode as a decrease in the maximum and increase in the broadness of the (002) peak is observed in the graphene components (Supplementary Figure S5a-b). Also, an increase in the peak maximum and broadness is observed for the (002) peak corresponding to RG in RG@RGNS composite due to the decrease in the interlayer distance, the introduction of disorder, and loss in the crystallinity of the graphitic domain with cycling

(Supplementary Figure S5c) which further blocks the passage of  $\text{Li}^+$ , decreases ion diffusivity and results in the trapping of the ions.

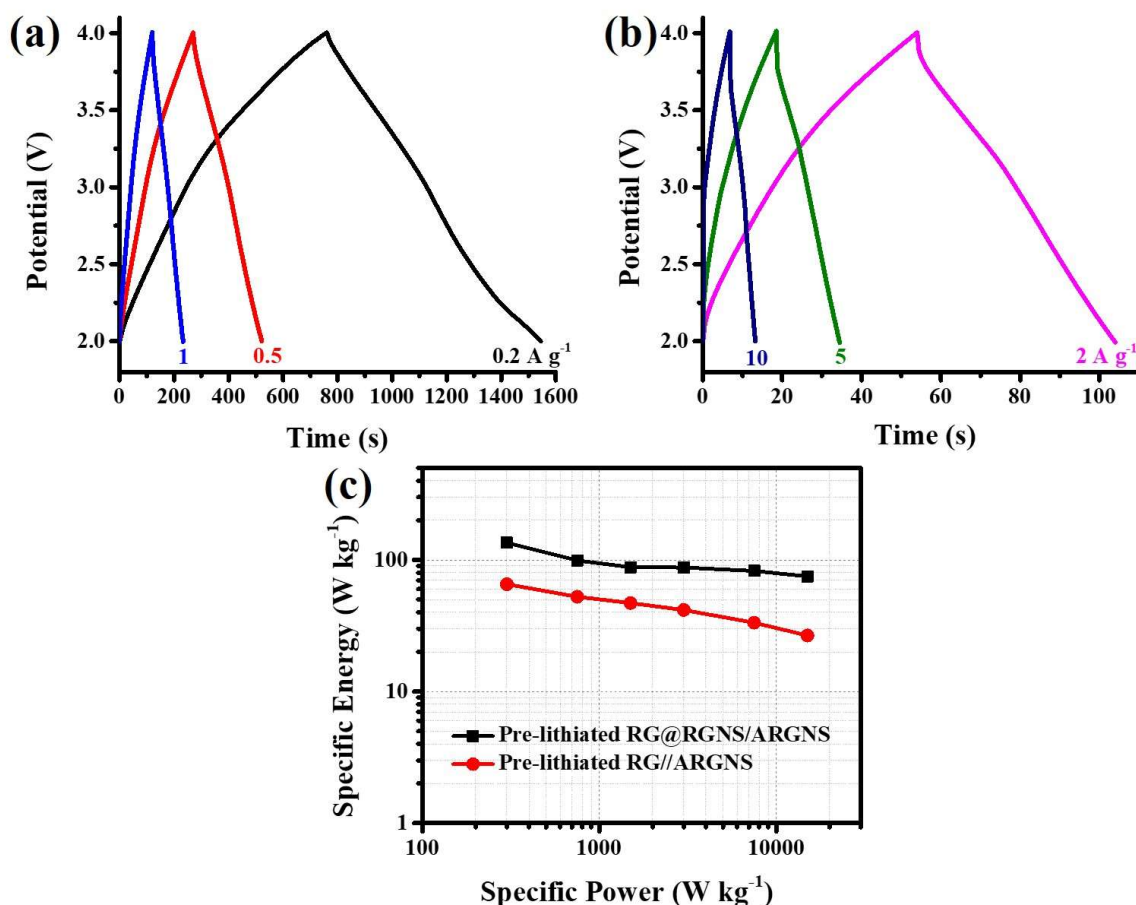


**Supplementary Figure S6:** Galvanostatic charge-discharge plot at different current densities (0.2, 0.5, 1, 2, 5, and 10  $\text{A g}^{-1}$ )



**Supplementary Figure S7:** 3-electrode analysis of the pre-lithiated RG@RGNS//ARGNS full cell at a current density of  $1 \text{ A g}^{-1}$ .

A 3-electrode setup is used to measure the potential evolution of the full-cell as well as individual cathode and anode versus  $\text{Li}/\text{Li}^+$  when a current density of  $1 \text{ A g}^{-1}$  is applied in the potential range of 2.0-4.0 V. The potential evolution at the anode reaches a minimum of  $\sim 0.01 \text{ V}$  and does not go below  $0.0 \text{ V}$  vs.  $\text{Li}/\text{Li}^+$ . This, in turn, discards any possibility of lithium plating.



**Supplementary Figure S8:** (a), (b) The galvanostatic charge-discharge cycling at different current densities, and (c) Comparative specific energy-power relation of pre-lithiated RG//ARGNS LIC full cell.

A full cell is fabricated using pre-lithiated recycled graphite (RG) as an anode and activated recycled graphene nanosheets (ARGNS) as a cathode in a 1:1 mass ratio. The pre-lithiated RG//RGNS full cell could deliver capacitances of 78.5, 63, 56.5, 50, 40, and 32  $\text{F g}^{-1}$  at current densities of 0.2, 0.5, 1, 2, 5, and 10  $\text{A g}^{-1}$ , respectively. Further, the full cell could deliver an energy

density of 65.5 Wh kg<sup>-1</sup> at a power density of 300 W kg<sup>-1</sup>. The full cell could retain an energy density of 32 Wh kg<sup>-1</sup> at a high power density of 15000 W kg<sup>-1</sup>. Thus, considerable improvement in deliverable capacitance and energy densities is observed when the recycled graphite is composited with recycled graphene.

*Supplementary Table 1: Comparison of RG@RGNS//ARGNS LIC with previously reported literature*

Device Configuration (Anode//Cathode)	Voltage	Energy (Whkg <sup>-1</sup> ) @ Power (Wkg <sup>-1</sup> )	Cycle life and retention	References
Graphite//AC	1.5-5V	145.8@65 18@18000	65% after 10K cycles	[2]
Graphene//AC	2-4V	95@27 61.5@222	75% after 300 cycles	[3]
Graphite// graphene	2-4V	135@50 105@1500	97% after 3.5K	[4]
Graphite// Functionalized graphene	2-4V	106@84 85@4200	100% after 1K cycles	[5]
Recycled graphite//AC	2-4.3 V	112@300	70% after 5K cycles	[6]
Recycled graphite//AC via diglyme co-intercalation	1.3-3.8V	46.4@248	>100% after 4K cycles @3 A g <sup>-1</sup>	[7]
DMF washed recycled graphite// AC	1.8-4.3V	185.5@319	75% after 2K cycles	[8]
<b>RG@RGNS//ARGNS</b>	<b>2.0-4V</b>	<b>135@300</b> <b>74@15000</b>	<b>70% after 10,000 cycles</b>	<b>In this work</b>

## References:

- [1] S. Ardizzzone, G. Fregonara, S. Trasatti, *Electrochimica Acta* 35 (1990) 263–267.
- [2] V. Khomenko, E. Raymundo-Piñero, F. Béguin, *Journal of Power Sources* 177 (2008) 643–651.
- [3] J.J. Ren, L.W. Su, X. Qin, M. Yang, J.P. Wei, Z. Zhou, P.W. Shen, *Journal of Power Sources* 264 (2014) 108–113.
- [4] J.H. Lee, W.H. Shin, S.Y. Lim, B.G. Kim, J.W. Choi, *Materials for Renewable and Sustainable Energy* 3 (2014) 1–8.
- [5] J.H. Lee, W.H. Shin, M.-H. Ryou, J.K. Jin, J. Kim, J.W. Choi, *ChemSusChem* 5 (2012) 2328–2333.
- [6] V. Aravindan, S. Jayaraman, F. Tedjar, S. Madhavi, *ChemElectroChem* 6 (2019) 1407–1412.
- [7] M.L. Divya, Y.-S. Lee, V. Aravindan, *Batteries & Supercaps* 4 (2021) 671–679.
- [8] M. L. Divya, S. Natarajan, Y.-S. Lee, V. Aravindan, *Journal of Materials Chemistry A* 8 (2020) 4950–4959.